Molecular Vision 2022; 28:57-69 <http://www.molvis.org/molvis/v28/57>
Received 18 December 2021 | Accepted 15 May 2022 | Published 17 May 2022

Novel *SIX6* mutations cause recessively inherited congenital cataract, microcornea, and corneal opacification with or without coloboma and microphthalmia

Evangelia S. Panagiotou,[1] Narcis Fernandez-Fuentes,[2] Layal Abi Farraj,[1] Martin McKibbin,[1,3] Nursel H. Elçioglu,[4,5] Hussain Jafri,[6] Eren Cerman,[7] David A. Parry,[1] Clare V. Logan,[1] Colin A. Johnson,[1] Chris F. Inglehearn,[1] Carmel Toomes,[1] Manir Ali[1]

(The last two authors contributed equally to the conduct of this research.)

[1]Division of Molecular Medicine, Leeds Institute of Medical Research, University of Leeds, United Kingdom; [2]Institute of Biological, Environmental & Rural Sciences, Aberystwyth University, United Kingdom; [3]Eye Clinic, St. James's University Hospital, Leeds, United Kingdom; [4]Department of Pediatric Genetics, Marmara University Medical School, Istanbul, Turkey; [5]Eastern Mediterrean University of Medical School, Cyprus, Turkey; [6]Fatima Jinnah Medical University, Lahore, Pakistan; [7]Department of Ophthalmology, Marmara University Medical School, Istanbul, Turkey

Purpose: To investigate the molecular basis of recessively inherited congenital cataract, microcornea, and corneal opacification with or without coloboma and microphthalmia in two consanguineous families.
Methods: Conventional autozygosity mapping was performed using single nucleotide polymorphism (SNP) microarrays. Whole-exome sequencing was completed on genomic DNA from one affected member of each family. Exome sequence data were also used for homozygosity mapping and copy number variation analysis. PCR and Sanger sequencing were used to confirm the identification of mutations and to screen further patients. Evolutionary conservation of protein sequences was assessed using CLUSTALW, and protein structures were modeled using PyMol.
Results: In family MEP68, a novel homozygous nucleotide substitution in *SIX6* was found, c.547G>C, that converts the evolutionarily conserved aspartic acid residue at the 183rd amino acid in the protein to a histidine, p.(Asp183His). This residue mapped to the third helix of the DNA-binding homeobox domain in SIX6, which interacts with the major groove of double-stranded DNA. This interaction is likely to be disrupted by the mutation. In family F1332, a novel homozygous 1034 bp deletion that encompasses the first exon of *SIX6* was identified, chr14:g.60975890_60976923del. Both mutations segregated with the disease phenotype as expected for a recessive condition and were absent from publicly available variant databases.
Conclusions: Our findings expand the mutation spectrum in this form of inherited eye disease and confirm that homozygous human *SIX6* mutations cause a developmental spectrum of ocular phenotypes that includes not only the previously described features of microphthalmia, coloboma, and congenital cataract but also corneal abnormalities.

Developmental eye defects such as microphthalmia, anophthalmia, and coloboma (MAC) are often associated with a spectrum of ocular phenotypes that involve the cornea, lens, iris, optic nerve, or retina [1]. Although often difficult to determine, these additional features could represent the primary defect or they may be secondary to the underlying MAC phenotype. These conditions are genetically heterogeneous and can affect common developmental pathways including transcription factor activity, TGFβ/BMP, and retinoic acid signaling [2].

Correspondence to: Manir Ali, Division of Molecular Medicine, Leeds Institute of Medical Research, University of Leeds, Wellcome Trust Brenner Building, St. James's University Hospital, Leeds LS9 7TF, UK; Phone: 44 113 343 8420; FAX: 44 113 343 8603; email: m.ali@leeds.ac.uk

Sine oculis homeobox homolog 6 (*SIX6*; OMIM 606326) is a 2-exon gene that translates into a 246 amino acid protein and belongs to a family of evolutionarily conserved transcription factors (SIX1-SIX6) that all originated by gene duplication and divergence from a common ancestor [3]. It has a protein-interacting SIX1_SD domain that forms complexes with cofactors to mediate transcriptional regulation, and a helix-turn-helix structural homeobox domain that binds DNA. To date, only four studies have reported *SIX6* mutations associated with recessively inherited eye disease in humans [4-7]. Two studies [4,5] reported a 5 bp homozygous deletion in *SIX6*, c.532_536del, that created a frameshift mutation, p.(Asn178Profs), which would be expected to lead to a null phenotype since part of the homeobox domain and the C-terminal end of the protein would be lost. Aldahmesh

et al. [4] identified this mutation in two siblings affected with microphthalmia associated with anterior and posterior segment abnormalities, although there was no evidence of coloboma. The younger child at 16 months of age had buphthalmos, corneal scarring, optic nerve cupping, and retinal detachment in the right eye and an extremely small globe without retinal detachment in the left eye. His 5-year-old sibling had bilateral retinal dystrophy and optic nerve dysplasia. More recently, Deepthi et al. [5] described this mutation in two affected brothers, suggesting a common founder effect. The younger child at 10 years old had anophthalmia of the right eye and microphthalmia, sclerocornea, and cataract but no coloboma in the left eye. The older sibling examined at 11.5 years old had bilateral anophthalmia, severe psychomotor delay, and intellectual disability. In another report, Yariz et al. [6] described a homozygous nucleotide substitution in *SIX6*, c.110T>C, that changed a leucine at the 37th amino acid in the protein to a proline, p.(Leu37Pro). This leucine residue is located in the SIX1_SD transactivation domain, which binds other nuclear proteins and is required for the DNA-binding activity of SIX6. The mutation to a proline residue disrupts this interaction, preventing optimal SIX6 function in the patient. This mutation was found in three affected children, aged 14, 5, and 2, of a consanguineous family that had iris and chorioretinal colobomas with macular atrophy and optic disc anomalies but without microphthalmia and cataracts. Additionally, Rudilla et al. [7] identified a 38-year-old male with congenital cataracts, strabismus, color blindness, and severe coloboma who had a homozygous *SIX6* variant, c.86G>C, that changed the evolutionary-conserved 29th amino acid located in the transactivation domain from an arginine to a proline, p.(Arg29Pro). This mutation is likely to affect normal function by disrupting the interaction of SIX6 with other proteins and reducing its capacity to bind DNA. Here, we report previously undescribed mutations in *SIX6* in two consanguineous families, allowing us to expand the mutation spectrum and clinical phenotype associated with this gene.

METHODS

Patient recruitment: This study was approved by the Leeds East Research Ethics Committee (project numbers 03/362 and 17/YH/003) and adhered to the tenets of the Declaration of Helsinki. Informed consent was obtained from all adult participants. In total, four affected (one male and three females) and three unaffected (two males and one female) subjects were recruited. Pedigree structures are depicted in Figure 1. The families were assessed by an experienced ophthalmologist and found to have no other obvious abnormalities apart from problems with their vision. Blood samples were obtained from both affected and unaffected family members where available, and genomic DNA was extracted using standard procedures. Genomic DNA from a panel of 196 patients with various ocular developmental phenotypes spanning the MAC spectrum were gathered from local, national, and international collaborations.

Autozygosity mapping: Whole-genome homozygosity mapping was performed using Affymetrix 6.0 SNP arrays (AROS Applied Biotechnologies, Aarhus, Denmark). The data were analyzed and presented using AgileMultiIdeogram software.

Whole-exome sequencing: Genomic DNA was processed according to Agilent's SureSelectQXT Library Prep protocol (Agilent Technologies Limited, Wokingham, UK) to enrich exonic regions using SureSelect All Exon V5 capture reagent. The processed libraries were subjected to 100 bp paired-end sequencing on a HiSeq2500 (Illumina, Little Chesterford, UK). The resulting reads were aligned to the human reference genome (GRCh37, hg19) using Novoalign short-read alignment software and processed in the SAM/BAM format using Picard and the Genome Analysis Toolkit (GATK) [8-10]. SNPs and indels were called in the variant call format using the HaplotypeCaller function of GATK. Variants were excluded if they were located outside the exons and flanking splice site regions, had a read depth of ≤10, were synonymous, or had a minor allele frequency >1% in EVS, 1000 Genomes, or gnomAD databases. The remaining variants were annotated using ANNOVAR software (version July 2014) [11]. To predict the pathogenicity of missense variants, PolyPhen2, Mutation Taster, and scaled CADD scores (Combined Annotation Dependent Depletion, version 1.3) were investigated.

ExomeDepth [12] and Integrative Genomics Viewer (IGV) were used to detect copy number variations in exome data. To check for homozygous regions in the exome data, the sequence variants were analyzed using AgileVariantMapper and presented as a MultiIdeogram.

Sanger DNA sequencing: Specific primer pairs used for PCR amplification and direct sequencing of the coding regions and flanking splice sites of *SIX6*, as well as the identification of the deletion breakpoint, were designed using Primer3 and are listed in Appendix 1. An aliquot of the PCR was checked for a product using agarose gel electrophoresis. The remaining product was digested with ExoSAP-IT (GE Healthcare, Freiburg, Germany) and sequenced using a BigDye Terminator v3.1 Cycle Sequencing Kit (Applied Biosystems). The sequencing reactions were resolved using an ABI3130xl Genetic Analyzer according to the manufacturer's instructions (Applied Biosystems).

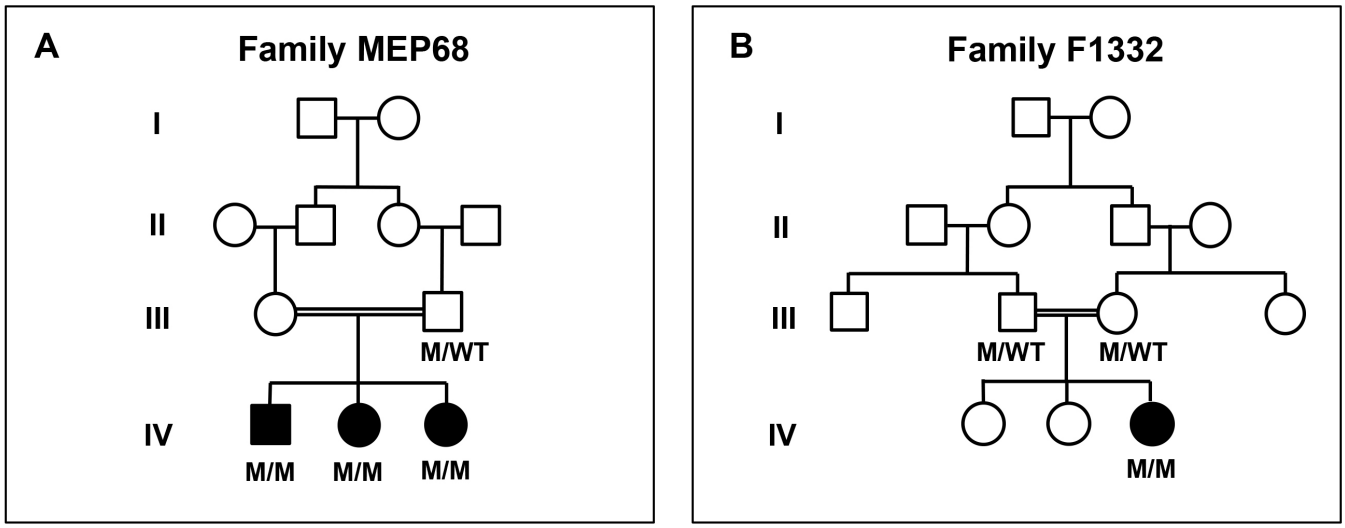

Figure 1. Pedigrees of the two families with affected members who have poor vision due to anterior eye abnormalities. **A**: Family MEP68. **B**: Family F1332. The genotypes for all tested family members from whom DNA was available are shown below each individual. M/M represents the homozygous mutant genotype, and M/WT represents the heterozygous genotype. Affected individuals are shaded black.

Bioinformatics: Protein sequences were downloaded from the National Center for Biotechnology Information (NCBI) databases. The conservation of amino acids was assessed by aligning protein sequences from different species using CLUSTALW.

Molecular modeling: The structural model of human SIX6 protein (Uniprot accession number O95475) was derived by homology modeling using M4T [13,14]. The crystal structure of the human SIX1-EYA2 protein complex [15] and the crystal structure of human Brn-5 transcription factor in complex with DNA [16] were used as templates. The mutation of the residue was modeled using Dunbrack's rotamer-dependent library. The quality and stereochemistry of the model were assessed using Prosa-II and PROCHECK and represented using PyMol.

RESULTS

Clinical phenotype of patients: Two families, one from Pakistan (MEP68) and the other from Turkey (F1332), were investigated in this study. The Pakistani family had previously been partly described by Khan et al. [17]. Three members of this family affected with visual impairment since early childhood were all clinically examined in their fifth decade. Two of the three individuals (Figure 1A, IV:1 & IV:3 and Table 1) had nystagmus and low vision (could count fingers only). Both had microcornea with corneal vascularization, peripheral corneal opacity, and cataract (Figure 2A). One of them (IV:1) also had iris coloboma. Indirect ophthalmoscopy showed no fundus abnormalities. The other affected member in this family (IV:2) had sclerocornea totalis, which prevented fundus viewing. Ocular ultrasound was not available, so the axial length of each eye could not be ascertained. The proband in the Turkish family (Figure 1B, IV:3, and Table 1) was diagnosed at the age of 1 with bilateral microphthalmia, corneal vascularization, sclerocornea, congenital cataract, and reduced/absent fundus reflexes. Follow-up at three years old showed microphthalmia, sclerocornea totalis with cornea plana, and flat anterior chambers (Figure 2B). B-scan ultrasonography revealed no posterior segment anomalies. Clinical examination of the affected cases from both families found no neurologic or other systemic abnormalities. The family history and evidence of consanguinity suggested autosomal recessive inheritance (Figure 1).

Molecular genetic analysis of family MEP68: To identify the causative mutation in this family, genomic DNA from two affected cases, IV:1 and IV:3, were analyzed by conventional autozygosity mapping using SNP microarrays. Several homozygous regions on chromosomes 1, 6, 7, 8, 11, 13, 14, and 20 were shared between both individuals (Figure 3A). To identify the pathogenic mutation, DNA from patient IV:1 was whole-exome sequenced. The resulting dataset of 63,009 variants that differed from the human genome reference assembly GRCh37, hg19, was filtered to select variants present at less than 1% in the public databases and that altered the protein-coding sequence or consensus splice signal of genes. Of these, only five homozygous variants, as listed in Table 2, mapped within the autozygous regions. Pathogenicity prediction software prioritized three of these variants (*GPR137, SIX6,*

Table 1. Clinical information of patients with poor vision due to biallelic *SIX6* mutations.

	Family ID	Ethnicity	Function	Globe	Cornea	Iris	Lens	Fundus	Mutation	Reference
A										
	MEP68 n=3	Pakistani	CF nystagmus	-	Microcornea Opacity/Sclerocornea Vascularization	Coloboma	Cataract	Normal	c.547G>C p.(Asp183His)	This paper
	F1332 n=1	Turkish	LP	Microphthalmia	Sclerocornea totalis Cornea plana Vascularization	-	Cataract	[Normal ultrasound]	c.-227_572+235del1034	This paper
B										
	n=2	Syrian	No LP	Microphthalmia Buphthalmos	Opacity	-	nd	Retinal dystrophy Optic disc dysplasia [Retinal detachment & Optic disc cupping ultrasound]	c.532_536del; p.(Asn178fs)	[4]
	n=2	Syrian	nd	Anophthalmia Microphthalmia	Sclerocornea	-	Cataract	nd	c.532_536del; p.(Asn178fs)	[5]
	n=3	Turkish	Low vision, nystagmus	-	nd	Coloboma	-	Pigmented macular atrophy Optic disc coloboma Chorioretinal coloboma Peri-papillary chorio-retinal changes	c.110T>C; p.(Leu37Pro)	[6]
	n=1	nd	Colour blindness, strabismus	nd	nd	nd	Cataract	Severe coloboma	c.86G>C; p.(Arg29Pro)	[7]

Details of patients reported in this study are presented (**A**) as well as patients previously documented to have biallelic SIX6 mutations (**B**). n=number of affected patients studied in each report, CF=count fingers, LP=light perception, -=no evidence of abnormality, nd=not documented. The references that report the mutations/affected cases are indicated. Note sclerocornea totalis makes visual fundus examination difficult. Also the use of B-scan ultrasonography for fundus inspection will detect only gross structural abnormalities in the retina and optic nerve rather than more subtle retinal atrophic changes.

and *ARHGAP40*) for further study based on their potential to be disease-causing. These variants were investigated in the genomic DNA of family members by Sanger sequencing to check for segregation of the alleles. Only the missense variant in *SIX6* (NM_007374: c.547G>C: p.(Asp183His)); ClinVar accession SCV000928400.1) segregated in the family as expected for a recessively-inherited condition (Figure 1A). This nucleotide substitution, which is not present in the EVS, 1000 Genomes, or gnomAD databases, is predicted to convert the evolutionarily conserved 183rd amino acid from an aspartic acid to a histidine (Figure 3B,C). The aspartic acid residue maps to the homeobox domain in SIX6. Modeling the DNA binding of SIX6 shows that the aspartic acid residue, which is negatively charged, is located in the third helix, also

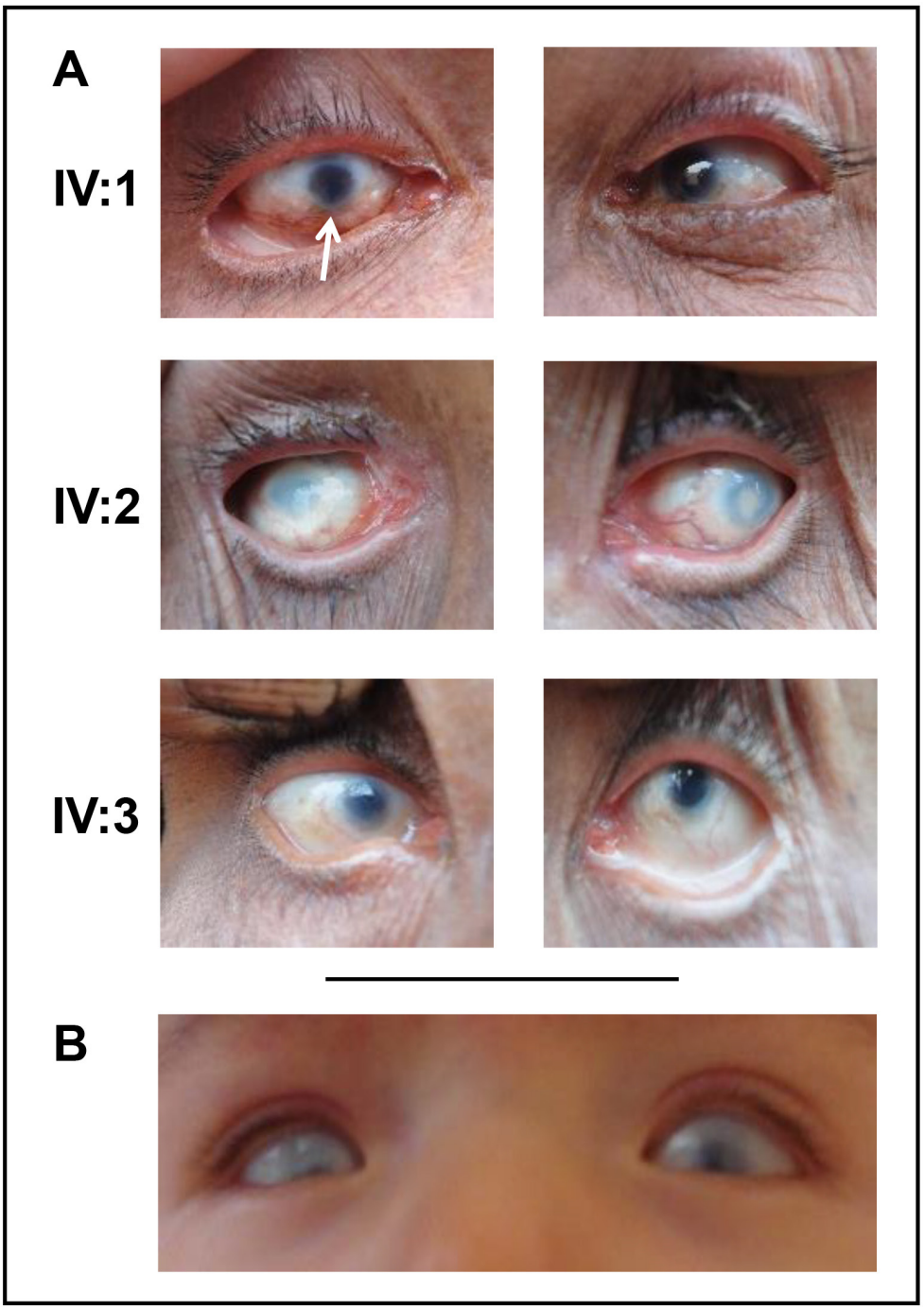

Figure 2. Anterior eye photos of affected members in this study. Images of the anterior segment of both eyes of patients IV:1 (aged 48 years), IV:2 (aged 46 years), and IV:3 (aged 42 years) from family MEP68 (A), and the proband (aged 1 year) from family F1332 (**B**). Note microcornea (A, IV:1 & IV:3), peripheral corneal opacity (**A**, IV:1 & IV:3), sclerocornea totalis (**A**, IV:2 & **B**), and iris coloboma (**A**, IV:1, right eye, arrowed).

called the recognition helix, and is in close contact with residues that directly interact with the major groove of double-stranded DNA. It seems likely that the histidine substitution, with its positively charged and bulkier imidazole side chain, disrupts the stabilization of the recognition helix, preventing normal protein function (Figure 3D).

Molecular genetic analysis of family F1332: To find the molecular basis of anterior segment anomalies and microphthalmia in the proband of family F1332, whole-exome sequencing was undertaken but failed to identify any homozygous variants in any of the known genes. A list of the known genes in which pathogenic variants had previously been found to cause nonsyndromic and syndromic MAC are shown in Appendix 2. As the presence of consanguinity does not preclude other patterns of inheritance, heterozygous variants were also analyzed. After filtering the exome variant list, 332 heterozygous variants remained with a read depth greater than 5, of which 113 were prioritized as candidates because they had a CADD score greater than 15 (Appendix 3), where a score of 20 or above was indicative of the variant being among the top 1% of deleterious changes in the human genome. Of the 113 heterozygous variants, none mapped to any of the known genes in which mutations had previously been implicated in MAC disease. Another possibility to consider was that there might be a mutation in a known gene not adequately covered during exome analysis. Mutations in forkhead box E3 (*FOXE3;* OMIM 601094) [18,19] cause a phenotype similar to that in the patient described here, yet it is often not well covered during exome sequencing, and the mutation may not be detected. However, the coding sequence of *FOXE3*, which maps to chr1:47,881,988–47,882,947 (GRCh37, hg19), was shown to be suitably covered in the exome sequence of the proband. The region 47,881,903 to 47,883,084 on chromosome 1, which contains *FOXE3*, was shown to have an average read count of 28.48 for each nucleotide, with 93.1% of the region above read count 10 and 99.9% above read count 5.

To detect any large copy number changes that would have been missed using the variant analysis filtering pipeline, ExomeDepth software was used on the exome dataset. This approach compared the read depth of each exon of

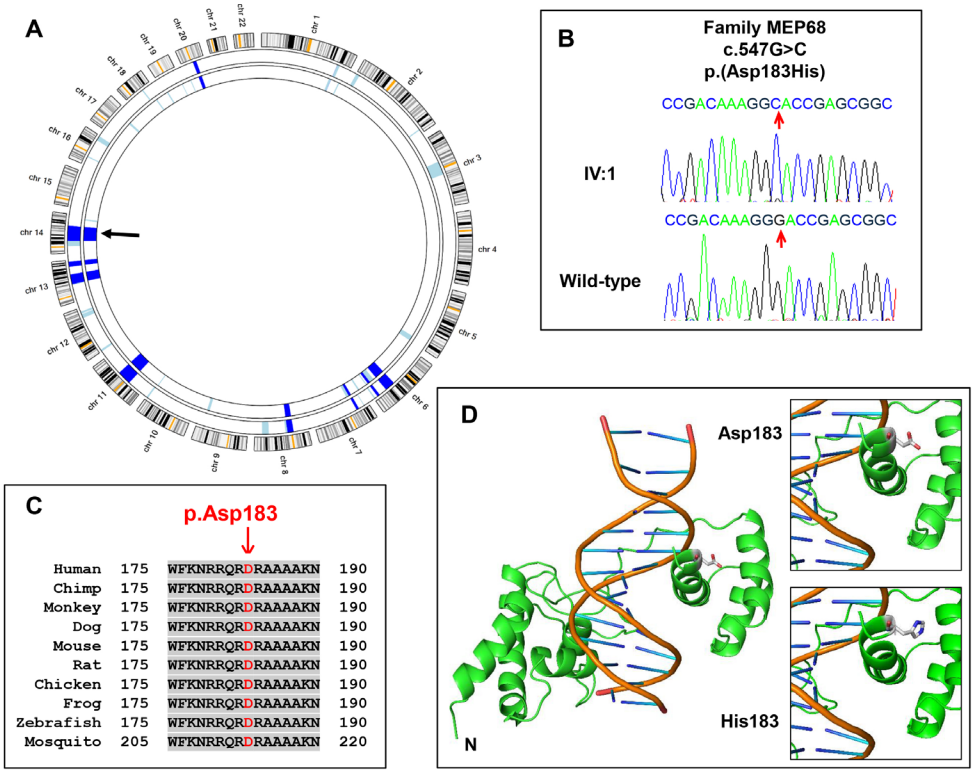

Figure 3. Genetic analysis of family MEP68. **A**: AgileMultiIdeogram representation of the homozygous regions from SNP-genotyping data of two affected individuals (IV:1 & IV:3). Homozygous regions are highlighted in light blue, and common autozygous regions are highlighted in dark blue. *SIX6* (arrow) maps to a common 42 Mb homozygous region on chromosome 14 (33,856,948–75,827,741, GRCh37, hg19). **B**: Sequence electropherograms highlighting the nucleotide substitution mutation, c.547G>C, in an affected individual from the family and a normal control subject. **C**: Multiple protein sequence alignment of human SIX6 with orthologs surrounding the p.D183 residue. Accession numbers: human, NP_031400.2; chimp, XP_522870.3; monkey, XP_014999313.1; dog, XP_547840.3; mouse, NP_035514.1; rat, NP_001101502.1; chicken, NP_001376294; frog, NP_001093696.1; zebrafish NP_957399.1; mosquito, XP_003436640.1. **D**: Modeling of SIX6 wild-type and p.(Asp183His) mutant. Ribbon representation of the structural model of SIX6 protein (green) bound to DNA (orange). The N-terminus and the atom types at the 183rd residue (white=carbon; blue=nitrogen; red=oxygen) are highlighted. Note the location of the 183rd residue sitting in the major groove of double-stranded DNA. It is likely that the change from a negatively charged D183 amino acid in the wild-type sequence to a positively charged H183 in the mutant is likely to disrupt this protein-DNA interaction.

Table 2. List of homozygous variants identified after filtering the exome sequencing data from patient IV:1 of family MEP68.

Chr	Position	Gene	Coding Effect	Transcript Accession Code: Exon: cDNA change: Protein change	Read Depth	EVS	1000g	gnomAD	Poly-Phen2	Muta-tion Taster	CADD
6	108395543	OSTM1	Missense	NM_014028:exon1:c.A313G:p.(Ser105Gly)	62	0.000077	0	0.000152	0.001 (B)	N	13.08
6	155561703	TIAM2	Missense	NM_012454:exon15:c.G3208A:p.(Asp1070Asn)	16	0	0.0002	0.000138	0.004 (B)	N	14.67
11	64056081	GPR137	Missense	NM_001170880:exon6:c.A919G:p.(Ser307Gly), NM_001170881:exon6:c.A769G:p.(Ser257Gly), NM_020155:exon6:c.A919G:p.(Ser307Gly), NM_001170726:exon8:c.A1093G:p.(Ser365Gly)	22	0	0	0	0.348 (B)	DC	10.77
14	60976663	SIX6	Missense	NM_007374:exon1:c.G547C:p.(Asp183His)	27	0	0	0	0.999 (D)	DC	27.6
20	37263365	ARHGAP40	Missense	NM_001164431:exon6:c.G883A:p.(Ala295Thr)	21	0	0.000799	0	U	N	16.64

The chromosome, position, gene, coding effect, transcript accession number, exon, cDNA and protein changes, variant read depth, minor allele frequency in the Exome Variant Server, 1000 Genomes and gnomAD databases are shown as well as the PolyPhen2, Mutation Taster and CADD scores for the 5 homozygous variants. B=benign, D=possibly damaging, U=unknown, N=probably neutral, DC=probably. A CADD score of 20 or above indicates that the variant is among the top 1% of deleterious changes in the human genome. For the purposes of this study, variants with CADD scores greater than 15 were prioritised. Note 3 variants (*GPR137, SIX6* and *ARHGAP40*) were prioritised for further investigation based on the criteria of having at least one deleterious pathogenicity prediction score (highlighted in red).

the proband's exome to seven unrelated exomes that were prepared using the same targeted enrichment reagent and ran in the same lane on the sequencer. The analysis revealed a homozygous deletion at the *SIX6* locus (Figure 4A) that was shown using the Integrative Genomics Viewer to remove all of exon 1, as the proband showed no sequence read coverage at this position (Appendix 4). Homozygosity mapping with the exome data confirmed a 33 Mb homozygous region at chromosome 14 (Chr14: 56,142,480–89,338,619, GRCh37), which contains the *SIX6* gene (Figure 4B). To find the deletion breakpoints in the patient's genomic DNA, oligonucleotide primers were designed to amplify the flanking sequences spanning the mutation until a suitable primer pair was identified (Appendix 1). PCR and Sanger sequencing identified a homozygous 1034 bp deletion in the proband (chr14:g.60975890_60976923del, c.-227_572+235del1034; ClinVar accession SCV000929754.1) that removed all 572 coding base pairs of exon 1 as well as 227 bp of the 5′ UTR and 235 bp of the first intron of *SIX6* (Figure 4C). This mutation is likely to lead to the complete absence of SIX6 protein in the patient, as there is no downstream methionine in exon 2. PCR combined with agarose gel electrophoresis was used to confirm that both parents, who were asymptomatic, were carriers of the deletion mutation (Figure 4D).

Both exons of *SIX6* and their flanking sequences were sequenced in a panel of 196 patients with various developmental ocular phenotypes similar to the affected cases in families MEP68 and F1332, but no further mutations were found. The F1332 exon 1 deletion breakpoint PCR primers were also used to screen this panel, but no further deletions were identified.

DISCUSSION

Here, we present two families, each with a novel homozygous *SIX6* mutation that causes non-syndromic eye disease in humans. Previously, only three recessively inherited *SIX6* mutations had been described [4-7]. The mutations, which included null and missense alleles, were mapped schematically (Figure 5). A clinical comparison of the phenotypic presentation of patients with biallelic *SIX6* mutations showed that they present with a spectrum of ocular developmental defects that may or may not include microphthalmia, corneal defects, cataracts, iris coloboma, optic nerve anomalies, and retinal abnormalities (see Table 1). Due to the small number of affected cases that have been studied so far, it is difficult to determine whether there are any obvious genotype–phenotype correlations. Nevertheless, it appears that patients with null mutations (family F1332) [4,5] represent the more severe end of the developmental condition with microphthalmia and little or no light perception, while patients with missense changes in the protein (family MEP68) [6] only have reduced vision in the absence of microphthalmia, although more studies are required to support these initial observations. The lack of MAC spectrum features in MEP68 is worth noting, as it is a novel observation.

Animal studies of mice, fish, frogs, and flies have also pointed to a role for SIX6 in eye specification, eye size, and retinal development. *Six6* is expressed in the developing and adult retina, optic stalk, hypothalamus, and pituitary gland in mice [20]. Mice lacking Six6 have increased expression of cyclin-dependent kinase inhibitors causing hypoplasia of the retina and pituitary, as well as absence of the optic nerves and chiasm [21]. Such mice have also been shown to have reduced fertility due to decreased gonadotrophin-releasing hormone [22] and irregular circadian rhythms associated with abnormal development of the suprachiasmatic nucleus [23]. Knockdown of the *SIX6* ortholog, *six6b,* in zebrafish leads to a small eye phenotype due to an underdeveloped lens and reduced optic nerve diameter [24], whereas overexpression of the *SIX6* ortholog, *XOptx2,* in *Xenopus* embryos causes the development of large eyes [25]. Intriguingly, the *Drosophila SIX6* ortholog, *optix,* can induce ectopic eye development in nonretinal tissues [26]. These studies highlight overlapping features observed in human patients with *SIX6* mutations who also show anterior segment defects.

It is important to note that previous studies in humans have suggested that the haploinsufficiency of *SIX6* was the likely disease mechanism for mutations in this gene [27-32]. For example, large heterozygous interstitial deletions at chromosome 14q22-q23 that encompass *SIX6* have been found in cases of anophthalmia with other developmental abnormalities [27-32]. However, since those earlier reports, heterozygous mutations in *orthodenticle homeobox 2* (*OTX2*; OMIM 600037), which is 3.7 Mb proximal to *SIX6* and within the deleted regions, have been found in cases with anophthalmia and pituitary defects [33,34]. Furthermore, heterozygous mutations in bone morphogenetic protein 4 (*BMP4*; OMIM 112262), which is 6.6 Mb proximal to *SIX6*, have been identified in patients with ocular abnormalities and polydactyly [35], similar to those patients described with 14q22 deletion and polydactyly [31]. Another study described a heterozygous *SIX6* missense variant in a case of bilateral anophthalmia and pituitary anomalies, although the patient inherited the variant from her unaffected father, suggesting that the variant may be of unknown significance or that her mother also carried a *SIX6* mutation that was not identified [36].

Studies have also reported associations of single nucleotide polymorphisms (SNPs) around the *SIX6* locus

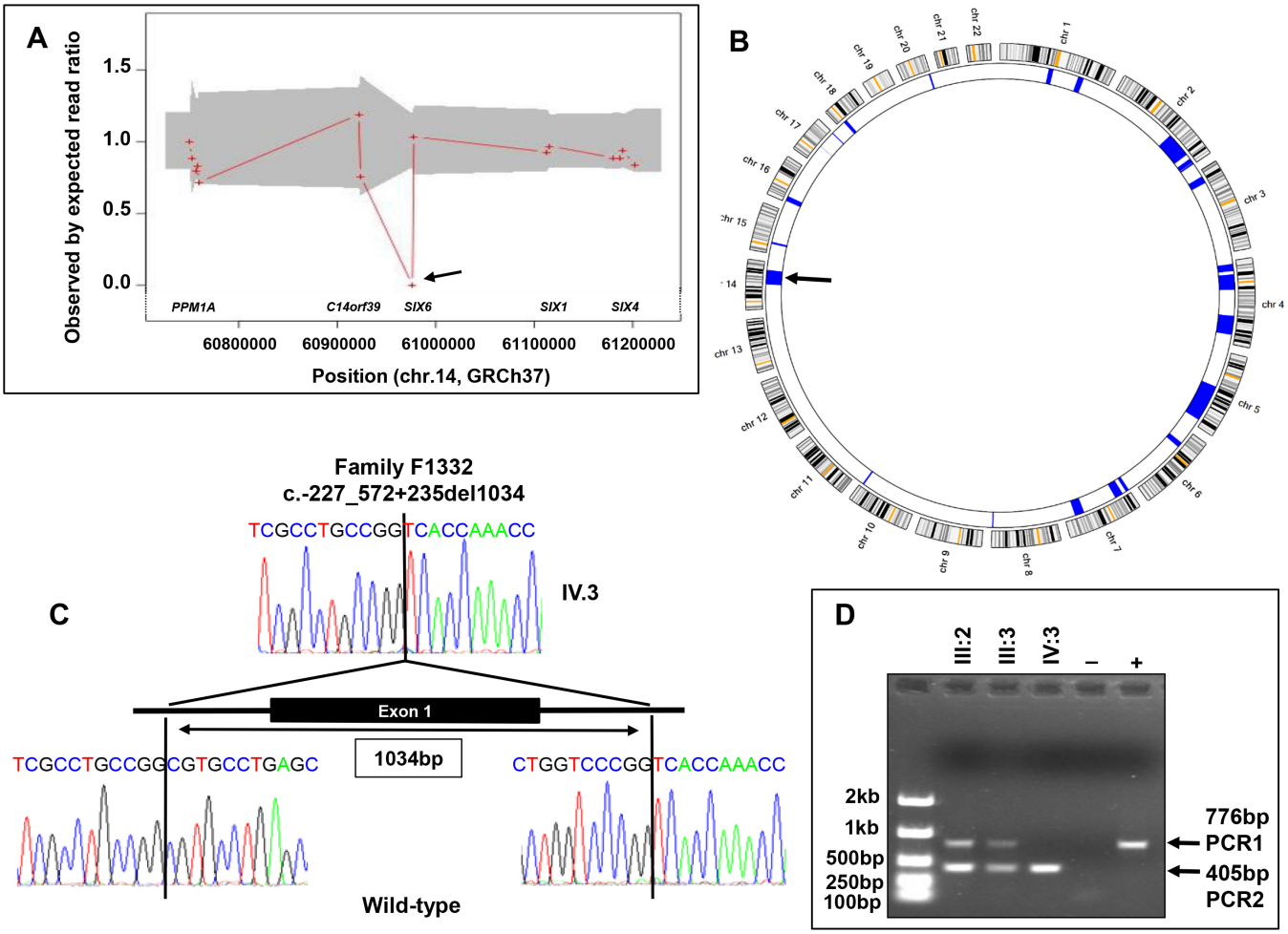

Figure 4. Genetic analysis of family F1332. **A**: ExomeDepth analysis of the proband's exome sequence data around the *SIX6* locus. The ratio of the observed (patient's exome data) to expected (seven unrelated control exomes) number of reads for each exon is indicated by a red cross, and the gray shaded region represents this ratio within 99% confidence intervals. Note that the majority of the ratios are around 1.0, although there is a single cross at 0.0 at the *SIX6* locus, suggesting a homozygous deletion in the proband (arrow). **B**: AgileMultiIdeogram derived from exome sequence data of the proband showing homozygous regions (in blue) against a circular ideogram of chromosomes 1 to 22. A 33 Mb homozygous region on chromosome 14 (56,142,480–89,338,619, GRCh37, hg19) spanning *SIX6* is shown (arrow). **C**: Sequence electropherogram highlights the junction of the deletion breakpoint in the proband. The deletion of 1034 bp removes exon 1 of *SIX6* and its surrounding sequences on either side. Sequence from a normal control subject is shown for comparison. **D**: PCR assay and agarose gel electrophoresis of additional family members. PCR1 and PCR2 were amplified in separate reaction mixtures, pooled in terms of patient order, and then run on the same gel. PCR1 gave a 776 bp product corresponding to a normal wild-type allele containing exon 1, whereas PCR2 would be expected to give a 405 bp product when the exon 1 deletion mutant allele was present. Note that the proband (IV:3) only gave a product of 405 bp for PCR2, confirming homozygosity for the deletion, whereas the parents (III:2 & III:3) gave products of 776 bp for PCR1 and 405 bp for PCR2, indicating their carrier status.

in cohorts of studies on late-onset, multigenic condition, primary open-angle glaucoma in Caucasian [37-40] and East Asian [41-43] subjects. The associated SNPs at the *SIX6* locus have included an intergenic variant, rs10483727 (T/C; T-allele associated), that is located approximately 94 kb downstream of *SIX6* [37-39,41,42], a variant 4562 bp downstream of *SIX6*, rs12436579 (C/A; C-allele associated), [43] and one that changes an amino acid residue, rs33912345, (c.421C/A, p.(His141Asn)); C-allele associated) in *SIX6* [40,42,43]. Patients homozygous for the functional p.His141 risk allele were found to have a thinner retinal nerve fiber layer compared to patients homozygous for the non-risk p.Asn141 allele [40]. Transient transfection experiments of the p.His141 risk variant, when compared to the p.Asn141 variant, in isolated rat retinal ganglion cells showed increased transcription of the cell cycle regulator, *cyclin dependent*

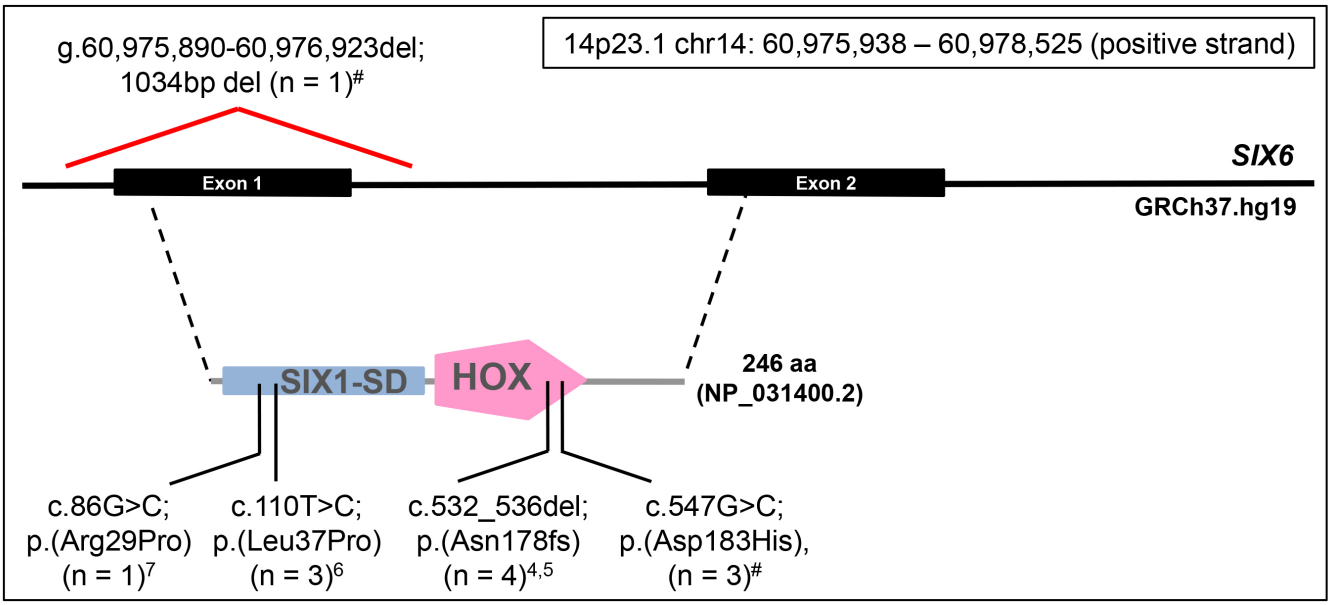

Figure 5. Diagrammatic representation of the *SIX6* genomic structure (GRCh37.hg19) and the 246 amino acid translated protein (NP_031400.2) with human mutations depicted. Note that the positions of the transactivation (SIX1_SD) and the homeobox (HOX) domains are shown. The positions of the *SIX6* mutations identified in recessive disease to date are also identified. The value of n denotes the number of related patients with that mutation, and the references that report the mutations are in superscript, with # indicating novel mutations identified in this report.

kinase inhibitor, CDKN2A isoform, INK4a (*p16INK4a*), and the senescence-associated secretory marker *interleukin 6* [44]. Similar experiments in cultured human fetal progenitor cells induced cell senescence that coincided with increased *p16INK4a* expression [44]. The authors concluded that increased *p16INK4a* expression, caused by promoter binding of the SIX6 p.His141 variant, causes retinal ganglion cells to senescence and consequently leads to cell death in glaucoma. The p.His141 risk allele has even been associated with thinner retinal nerve fiber layer in general population-based controls [45,46]. Based on these observations, it is worth highlighting that although the parents of the affected cases described here are heterozygous carriers for a *SIX6* mutation and do not show any obvious ocular symptoms following clinical examination, they might be at increased risk of developing late-onset glaucoma.

To summarize, we report previously undescribed mutations in the gene *SIX6* as the cause of the ocular phenotype in two consanguineous families. The phenotype includes congenital cataract and various corneal defects (opacity, microcornea, sclerocornea, and cornea plana) in the presence or absence of iris coloboma and microphthalmia. This report not only increases the spectrum of *SIX6* mutations in this form of eye disease but also reports corneal abnormalities as part of the phenotype.

APPENDIX 1. PRIMERS FOR THE PCR AND SANGER SEQUENCING OF SIX6.

To access the data, click or select the words "Appendix 1." The names, DNA sequences of each primer and PCR product size(s) are shown. Note the SIX6-Exon1-deletion PCR sizes correspond to the expected 405bp for the exon 1 deleted allele.

APPENDIX 2. LIST OF 102 KNOWN GENES IN WHICH PATHOGENIC MUTATIONS CAUSE ALL FORMS OF MAC DISEASE.

To access the data, click or select the words "Appendix 2." The gene name, OMIM entry number, inheritance pattern in human disease and whether mutation causes non-syndromic, or syndromic, MAC are indicated. The 102 gene list was derived from the Gene Vision website (https://gene.vision/knowledge-base/microphthalmia-anophthalmia-coloboma-for-doctors/#genetics). AR = autosomal recessive, AD = autosomal dominant, XL = X-linked, XLR = X-linked recessive, XLD = X-linked dominant, NS = nonsyndromic disease involving the eyes only and S = syndromic disease affecting the eyes and other organs also.

APPENDIX 3. THE 113 HETEROZYGOUS VARIANTS IDENTIFIED WITH A READ COUNT >5 AND CADD SCORE >15 AFTER FILTERING THE EXOME SEQUENCING DATA OF PATIENT IV:3 FROM FAMILY F1332.

To access the data, click or select the words "Appendix 3." The chromosome, position, gene, coding effect, transcript accession number, exon, cDNA and protein changes, variant read depth, minor allele frequency in the Exome Variant Server and 1000 Genomes databases are shown as well as the PolyPhen2, Mutation Taster and CADD scores for the 113 heterozygous variants. B = benign, D = possibly damaging, N = probably neutral, DC = probably disease-causing. Note there are no variants in any of the known genes (listed in Appendix 2) in which mutations have previously been found to be associated with a MAC phenotype.

APPENDIX 4. INTEGRATIVE GENOMICS VIEWER OF WHOLE EXOME SEQUENCE FROM THE PROBAND OF FAMILY F1332 AT THE SIX6 LOCUS.

To access the data, click or select the words "Appendix 4." The chromosome 14 banding pattern, location from the top of the chromosome and the SIX6 gene locus (in blue) are shown. The coverage track above the reads represents depth of coverage for all reads and the grey bars depict individual sequence reads. Note that exon 2 is fully covered with multiple reads whereas there are no reads (in red) covering exon 1.

ACKNOWLEDGMENTS

Funding for the work described in this manuscript was provided by the European Union's Seventh Framework Programme for research, technological development, and demonstration under agreement no. 317472 (EyeTN). ESP was an EU Early Stage Researcher (grant number 317472) and LAF was a Fight for Sight PhD student (grant number 1835) during this work. NFF acknowledges support from the Biotechnology & Biological Sciences Research Council (BBSRC) (grant number BBS/E/W/0012843D), and CAJ and CFI were supported by a Sir Jules Thorn Charitable Trust Biomedical Award (grant number 09/JTA).

REFERENCES

1. Williamson KA, FitzPatrick DR. The genetic architecture of microphthalmia, anophthalmia and coloboma. Eur J Med Genet 2014; 57:369-80. [PMID: 24859618].

2. Reis LM, Semina EV. Conserved genetic pathways associated with microphthalmia, anophthalmia, and coloboma. Birth Defects Res C Embryo Today 2015; 105:96-113. [PMID: 26046913].

3. Seo HC, Curtiss J, Mlodzik M, Fjose A. Six class homeobox genes in Drosophila belong to three distinct families and are involved in head development. Mech Dev 1999; 83:127-39. [PMID: 10381573].

4. Aldahmesh MA, Khan AO, Hijazi H, Alkuraya FS. Homozygous truncation of six6 causes complex microphthalmia in humans. Clin Genet 2013; 84:198-9. [PMID: 23167593].

5. Deepthi A, Fakhoury O, Daher M, Gambarini A, El-Hayek S, Megarbane A. SIX6-related anophthalmia/microphthalmia: second report on a deletion in a consanguineous family. Ophthalmic Genet 2021; 42:88-91. [PMID: 33108933].

6. Yariz KO, Sakalar YB, Jin X, Hertz J, Sener EF, Akay H, Ozbek MN, Farooq A, Goldberg J, Tekin M. A homozygous six6 mutation is associated with optic disc anomalies and macular atrophy and reduces retinal ganglion cell differentiation. Clin Genet 2015; 87:192-5. [PMID: 24702266].

7. Rudilla F, Franco-Jarava C, Martínez-Gallo M, Garcia-Prat M, Martín-Nalda A, Rivière J, Aguiló-Cucurull A, Mongay L, Vidal F, Solanich X, Irastorza I, Santos-Pérez JL, Sánchez JT, Cuscó I, Serra C, Baz-Redón N, Fernández-Cancio M, Carreras C, Vagace JM, Garcia-Patos V, Pujol-Borrell R, Soler-Palacín P, Colobran R. Expanding the clinical and genetic spectra of primary immunodeficiency-related disorders with clinical exome sequencing: expected and unexpected findings. Front Immunol 2019; 10:2325-[PMID: 31681265].

8. Li H, Handsaker B, Wysoker A, Fennell T, Ruan J, Homer N, Marth G, Abecasis G, Durbin R. Genome Project Data Processing S. The sequence alignment/map format and samtools. Bioinformatics 2009; 25:2078-9. [PMID: 19505943].

9. DePristo MA, Banks E, Poplin R, Garimella KV, Maguire JR, Hartl C, Philippakis AA, del Angel G, Rivas MA, Hanna M, McKenna A, Fennell TJ, Kernytsky AM, Sivachenko AY, Cibulskis K, Gabriel SB, Altshuler D, Daly MJ. A framework for variation discovery and genotyping using next-generation DNA sequencing data. Nat Genet 2011; 43:491-8. [PMID: 21478889].

10. McKenna A, Hanna M, Banks E, Sivachenko A, Cibulskis K, Kernytsky A, Garimella K, Altshuler D, Gabriel S, Daly M, DePristo MA. The genome analysis toolkit: A mapreduce framework for analyzing next-generation DNA sequencing data. Genome Res 2010; 20:1297-303. [PMID: 20644199].

11. Wang K, Li M, Hakonarson H. Annovar: Functional annotation of genetic variants from high-throughput sequencing data. Nucleic Acids Res 2010; 38:e164-[PMID: 20601685].

12. Plagnol V, Curtis J, Epstein M, Mok KY, Stebbings E, Grigoriadou S, Wood NW, Hambleton S, Burns SO, Thrasher AJ, Kumararatne D, Doffinger R, Nejentsev S. A robust model for read count data in exome sequencing experiments and

implications for copy number variant calling. Bioinformatics 2012; 28:2747-54. [PMID: 22942019].

13. Fernandez-Fuentes N, Madrid-Aliste CJ, Rai BK, Fajardo JE, Fiser A. M4T: a comparative protein structure modeling server. Nucleic Acids Res 2007; 35:W363-8-[PMID: 17517764].

14. Fernandez-Fuentes N, Rai BK, Madrid-Aliste CJ, Fajardo JE, Fiser A. Comparative protein structure modeling by combining multiple templates and optimizing sequence-to-structure alignments. Bioinformatics 2007; 23:2558-65. [PMID: 17823132].

15. Patrick AN. Joshua H Cabrera, Anna L Smith, Xiaojiang S Chen, Heide L Ford, Rui ZhaoStructure-function analyses of the human SIX1–EYA2 complex reveal insights into metastasis and BOR syndrome. Nat Struct Mol Biol 2013; 20:447-53. [PMID: 23435380].

16. Pereira JH, Kim SH. Structure of human Brn-5 transcription factor in complex with CRH gene promoter. J Struct Biol 2009; 167:159-65. [PMID: 19450691].

17. Khan K, Al-Maskari A, McKibbin M, Carr IM, Booth A, Mohamed M, Siddiqui S, Poulter JA, Parry DA, Logan CV, Hashmi A, Sahi T, Jafri H, Raashid Y, Johnson CA, Markham AF, Toomes C, Rice A, Sheridan E, Inglehearn CF, Ali M. Genetic heterogeneity for recessively inherited congenital cataract microcornea with corneal opacity. Invest Ophthalmol Vis Sci 2011; 52:4294-9. [PMID: 21474777].

18. Iseri SU, Osborne RJ, Farrall M, Wyatt AW, Mirza G, Nürnberg G, Kluck C, Herbert H, Martin A, Hussain MS, Collin JRO, Lathrop M, Nürnberg P, Ragoussis J, Ragge NK. Seeing clearly: the dominant and recessive nature of FOXE3 in eye developmental anomalies. Hum Mutat 2009; 30:1378-86. [PMID: 19708017].

19. Ali M, Buentello-Volante B, McKibbin M, Rocha-Medina JA, Fernandez-Fuentes N, Koga-Nakamura W, Ashiq A, Khan K, Booth AP, Williams G, Raashid Y, Jafri H, Rice A, Inglehearn CF, Zenteno JC. Homozygous FOXE3 mutations cause non-syndromic, bilateral, total sclerocornea, aphakia, microphthalmia and optic disc coloboma. Mol Vis 2010; 16:1162-8. [PMID: 20664696].

20. Toy J, Sundin OH. Expression of the optx2 homeobox gene during mouse development. Mech Dev 1999; 83:183-6. [PMID: 10381579].

21. Li X, Perissi V, Liu F, Rose DW, Rosenfeld MG. Tissue-specific regulation of retinal and pituitary precursor cell proliferation. Science 2002; 297:1180-3. [PMID: 12130660].

22. Larder R, Clark DD, Miller NL, Mellon PL. Hypothalamic dysregulation and infertility in mice lacking the homeodomain protein six6. J Neurosci 2011; 31:426-38. [PMID: 21228153].

23. Clark DD, Gorman MR, Hatori M, Meadows JD, Panda S, Mellon PL. Aberrant development of the suprachiasmatic nucleus and circadian rhythms in mice lacking the homeodomain protein six6. J Biol Rhythms 2013; 28:15-25. [PMID: 23382588].

24. Iglesias AI, Springelkamp H, van der Linde H, Severijnen LA, Amin N, Oostra B, Kockx CE, van den Hout MC, van Ijcken WF, Hofman A, Uitterlinden AG, Verdijk RM, Klaver CC, Willemsen R, van Duijn CM. Exome sequencing and functional analyses suggest that SIX6 is a gene involved in an altered proliferation-differentiation balance early in life and optic nerve degeneration at old age. Hum Mol Genet 2014; 23:1320-32. [PMID: 24150847].

25. Zuber ME, Perron M, Philpott A, Bang A, Harris WA. Giant eyes in xenopus laevis by overexpression of xoptx2. Cell 1999; 98:341-52. [PMID: 10458609].

26. Seimiya M, Gehring WJ. The drosophila homeobox gene optix is capable of inducing ectopic eyes by an eyeless-independent mechanism. Development 2000; 127:1879-86. [PMID: 10751176].

27. Bennett CP, Betts DR, Seller MJ. Deletion 14(q22– q23) associated with anophthalmia, absent pituitary and other abnormalities. J Med Genet 1991; 28:280-1. [PMID: 1856837].

28. Elliott J, Maltby EL, Reynolds B. A case of deletion 14(q22.1q22.3) associated with anophthalmia and pituitary abnormalities. J Med Genet 1993; 30:251-2. [PMID: 7682620].

29. Lemyre E, Lemieux N, Decarie JC, Del Lambert M. (14)(q22.1q23.2) in a patient with anophthalmia and pituitary hypoplasia. Am J Med Genet 1998; 77:162-5. [PMID: 9605291].

30. Gallardo ME, Lopez-Rios J, Fernaud-Espinosa I, Granadino B, Sanz R, Ramos C, Ayuso C, Seller MJ, Brunner HG, Bovolenta P, Rodríguez de Córdoba S. Genomic cloning and characterization of the human homeobox gene SIX6 reveals a cluster of SIX genes in chromosome 14 and associates SIX6 hemizygosity with bilateral anophthalmia and pituitary anomalies. Genomics 1999; 61:82-91. [PMID: 10512683].

31. Ahmad ME, Dada R, Dada T, Kucheria K. 14q(22) deletion in a familial case of anophthalmia with polydactyly. Am J Med Genet 2003; 120A:117-22. [PMID: 12794703].

32. Nolen LD, Amor D, Haywood A, St Heaps L, Willcock C, Mihelec M, Tam P, Billson F, Grigg J, Peters G, Jamieson RV. Deletion at 14q22–23 indicates a contiguous gene syndrome comprising anophthalmia, pituitary hypoplasia, and ear anomalies. Am J Med Genet 2006; 140:1711-8. [PMID: 16835935].

33. Ragge NK, Brown AG, Poloschek CM, Lorenz B, Henderson RA, Clarke MP, Russell-Eggitt I, Fielder A, Gerrelli D, Martinez-Barbera JP, Ruddle P, Hurst J, Collin JRO, Salt A, Cooper ST, Thompson PJ, Sisodiya SM, Williamson KA, Fitzpatrick DR, van Heyningen V, Hanson IM. Heterozygous mutations of OTX2 cause severe ocular malformations. Am J Hum Genet 2005; 76:1008-22. [PMID: 15846561].

34. Tajima T, Ohtake A, Hoshino M, Amemiya S, Sasaki N, Ishizu K, Fujieda K. OTX2 loss of function mutation causes anophthalmia and combined pituitary hormone deficiency with a small anterior and ectopic posterior pituitary. J Clin Endocrinol Metab 2009; 94:314-9. [PMID: 18854396].

35. Bakrania P, Efthymiou M, Klein JC, Salt A, Bunyan DJ, Wyatt A, Ponting CP, Martin A, Williams S, Lindley V, Gilmore J, Restori M, Robson AG, Neveu MM, Holder GE, Collin JR, Robinson DO, Farndon P, Johansen-Berg H, Gerrelli D, Ragge NK. Mutations in BMP4 cause eye, brain, and digit developmental anomalies: overlap between the BMP4 and hedgehog signaling pathways. Am J Hum Genet 2008; 82:304-19. [PMID: 18252212].

36. Gallardo ME, Rodríguez De Córdoba S, Schneider AS, Dwyer MA, Ayuso C, Bovolenta P. Analysis of the developmental SIX6 homeobox gene in patients with anophthalmia/microphthalmia. Am J Med Genet 2004; 129A:92-4. [PMID: 15266624].

37. Fan BJ, Wang DY, Pasquale LR, Haines JL, Wiggs JL. Genetic variants associated with optic nerve vertical cup-to-disc ratio are risk factors for primary open angle glaucoma in a US Caucasian population. Invest Ophthalmol Vis Sci 2011; 52:1788-92. [PMID: 21398277].

38. Ramdas WD, van Koolwijk LM, Lemij HG, Pasutto F, Cree AJ, Thorleifsson G, Janssen SF, Jacoline TB, Amin N, Rivadeneira F, Wolfs RC, Walters GB, Jonasson F, Weisschuh N, Mardin CY, Gibson J, Zegers RH, Hofman A, de Jong PT, Uitterlinden AG, Oostra BA, Thorsteinsdottir U, Gramer E, Welgen-Lüssen UC, Kirwan JF, Bergen AA, Reis A, Stefansson K, Lotery AJ, Vingerling JR, Jansonius NM, Klaver CC, van Duijn CM. Common genetic variants associated with open-angle glaucoma. Hum Mol Genet 2011; 20:2464-71. [PMID: 21427129].

39. Wiggs JL, Yaspan BL, Hauser MA, Kang JH, Allingham RR, Olson LM, Abdrabou W, Fan BJ, Wang DY, Brodeur W, Budenz DL, Caprioli J, Crenshaw A, Crooks K, Delbono E, Doheny KF, Friedman DS, Gaasterland D, Gaasterland T, Laurie C, Lee RK, Lichter PR, Loomis S, Liu Y, Medeiros FA, McCarty C, Mirel D, Moroi SE, Musch DC, Realini A, Rozsa FW, Schuman JS, Scott K, Singh K, Stein JD, Trager EH, Vanveldhuisen P, Vollrath D, Wollstein G, Yoneyama S, Zhang K, Weinreb RN, Ernst J, Kellis M, Masuda T, Zack D, Richards JE, Pericak-Vance M, Pasquale LR, Haines JL. Common variants at 9p21 and 8q22 are associated with increased susceptibility to optic nerve degeneration in glaucoma. PLoS Genet 2012; 8:e1002654-[PMID: 22570617].

40. Carnes MU, Liu YP, Allingham RR, Whigham BT, Havens S, Garrett ME, Qiao C, Investigators NC, Katsanis N, Wiggs JL, Pasquale LR, Ashley-Koch A, Oh EC, Hauser MA. Discovery and functional annotation of six6 variants in primary open-angle glaucoma. PLoS Genet 2014; 10:e1004372-[PMID: 24875647].

41. Osman W, Low SK, Takahashi A, Kubo M, Nakamura Y. A genome-wide association study in the Japanese population confirms 9p21 and 14q23 as susceptibility loci for primary open angle glaucoma. Hum Mol Genet 2012; 21:2836-42. [PMID: 22419738].

42. Shiga Y, Nishiguchi KM, Kawai Y, Kojima K, Sato K, Fujita K, Takahashi M, Omodaka K, Araie M, Kashiwagi K, Aihara M, Iwata T, Mabuchi F, Takamoto M, Ozaki M, Kawase K, Fuse N, Yamamoto M, Yasuda J, Nagasaki M, Nakazawa T. Japan Glaucoma Society Omics Group (JGS-OG). Genetic analysis of Japanese primary open-angle glaucoma patients and clinical characterization of risk alleles near CDKN2B–AS1, SIX6 and GAS7. PLoS One 2017; 12:e0186678-[PMID: 29261660].

43. Rong SS, Lu SY, Matsushita K, Huang C, Leung CKS, Kawashima R, Usui S, Tam POS, Young AL, Tsujikawa M, Zhang M, Nishida K, Wiggs JL, Tham CC, Pang CP, Chen LJ. Association of the SIX6 locus with primary open angle glaucoma in southern Chinese and Japanese. Exp Eye Res 2019; 180:129-36. [PMID: 30586556].

44. Skowronska-Krawczyk D, Zhao L, Zhu J, Weinreb RN, Cao G, Luo J, Flagg K, Patel S, Wen C, Krupa M, Luo H, Ouyang H, Lin D, Wang W, Li G, Xu Y, Li O, Chung C, Yeh E, Jafari M, Ai M, Zhong Z, Shi W, Zheng L, Krawczyk M, Chen D, Shi C, Zin C, Zhu J, Mellon PL, Gao W, Abagyan R, Zhang L, Sun X, Zhong S, Zhuo Y, Rosenfeld MG, Liu Y, Zhang K. P16ink4a upregulation mediated by six6 defines retinal ganglion cell pathogenesis in glaucoma. Mol Cell 2015; 59:931-40. [PMID: 26365380].

45. Cheng CY, Allingham RR, Aung T, Tham YC, Hauser MA, Vithana EN, Khor CC, Wong TY. Association of common SIX6 polymorphisms with peripapillary retinal nerve fiber layer thickness: the Singapore Chinese Eye Study. Invest Ophthalmol Vis Sci 2014; 56:478-83. [PMID: 25537207].

46. Khawaja AP, Chan MPY, Yip JLY, Broadway DC, Garway-Heath DF, Viswanathan AC, Luben R, Hayat S, Hauser MA, Wareham NJ, Khaw KT, Fortune B, Allingham RR, Foster PJ. A Common glaucoma-risk variant of SIX6 alters retinal nerve fiber layer and optic disc measures in a European population: The EPIC-Norfolk Eye Study. J Glaucoma 2018; 27:743-9. [PMID: 30005032].

Articles are provided courtesy of Emory University and the Zhongshan Ophthalmic Center, Sun Yat-sen University, P.R. China. The print version of this article was created on 17 May 2022. This reflects all typographical corrections and errata to the article through that date. Details of any changes may be found in the online version of the article.